Paper No. ICMM2005-75228

Visualization of Convective Boiling Heat Transfer in Single Micro-Conduits with Different Shapes of Cross Sections

Tzu-Hsiang Yen[a], Masahiro Shoji[a], Fumio Takemura[a], Yuji Suzuki[b] and Nobuhide Kasagi[b]
[a]Energy Technology Research Institute, AIST, 1-2-1 Namiki, Tsukuba-shi, Ibaraki, 305-8564, Japan
[b]Department of Mechanical Engineering, The University of Tokyo,
Bunkyo-ku, Hongo 7-3-1, Tokyo, 113-8656, Japan

ABSTRACT

Visualization experiments of convective boiling in transparent single micro conduits with the same hydraulic diameter but different cross sections are carried out with simultaneous measurement of local heat transfer coefficients and pressure losses. Two different cross sections with the same similar hydraulic diameters are applied: A circular microtube of 210μm in diameter and a square microchannel of 214μmx 214μm cross section. ITO/Ag thin film of 100 nm is sputtered on the outer surface of the conduits for the direct joule heating.

The convective boiling shows some periodic variation of different flow patterns in both square and circular conduits. These flow patterns include bubbly, plug, slug, annular and capillary flows. The capillary flow pattern is the independent liquid droplets moving in the flow direction and very rarely observed in conventional tubes. The reason of such variation of flow patterns is that confined spaces limit the bubble growth in radial direction. So the nucleation bubble grows in both upstream and downstream and makes the flow pattern varies radically.

The square microchannel conduit has more simple flow pattern variation, more nucleation bubbles and larger local heat transfer coefficients at lower vapor quality. It is due to that corners of the square microchannel act as helps nucleation cavities. Corners also promotes the formation of liquid film and the contact line between liquid and wall, which can stabilize the flow field.

Local heat transfer coefficients decrease with increasing local vapor qualities. Local heat transfer coefficients increase with increasing boiling number but have their maximum value when boiling number reaches critical value. Such peculiar heat transfer characteristics can also be explained by the visualization results.

INTRODUCTION

Convective boiling heat transfer in microchannels has become an important issue for its high potential on electronic device cooling, highly efficient compact heat exchangers and reformers for methane direct micro fuel cells.

Recently, many research works focusing on boiling heat transfer in mini/micro conduits have been carried out. Ravigururajan (1998) measured the average heat transfer coefficient in parallel square microchannels of 0.425μm ID. Saitoh et al. (2000) employed 1.12 and 0.51 mm ID mini circular tubes with R-134a refrigerant, offering the local heat transfer coefficient data. Yen et al. (2003) measured the local heat transfer coefficients in single SUS 304 circular microtubes from 0.19~0.51 mm ID. Kandlikar (2004) measured the averaged heat transfer coefficients in parallel square microchannels of 0.2 mm ID. All the above experimental results above show the similar tendency: The heat transfer coefficient decreases with increasing vapor quality and very small dependence of the heat transfer coefficient to heat and mass fluxes at low heat and mass fluxes. However, the reasons for such above peculiar heat transfer characteristics need to be further studied.

Another problem rising from the research results concerning convective boiling in microchannels is the effect of cross section and surface roughness has been seldom studied. In pool boiling or convective boiling, it is widely known that the size and shape of nucleation cavities are the dominant parameters for bubble growth and heat transfer characteristics. Since in convective boiling of microchannels, nucleate boiling mechanism becomes much more dominant than convective boiling mechanism (Kandlikar, 2004, Yen et al., 2003), discussions of experimental data without exploring surface roughness are apparently insufficient. On the other hand, since there is still no experimental investigation covers both circular cross section and square cross section, in which the effect of corners can serve as very effective nucleation sites and controls the shape of liquid film, liquid-gas inter-phase
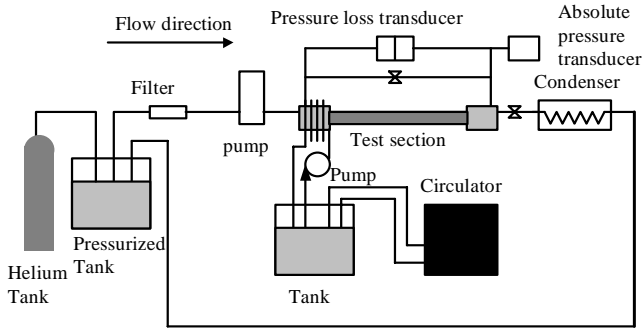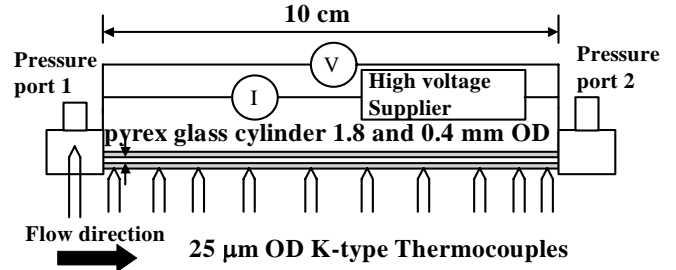
Fig. 1 Experimental loop

Fig. 2 Test section

Fig. 3 SEM Photo of thin ITO/Ag film of 100 nm in thickness is sputtered on the outer wall of the cylinder

Fig. 4 Visualization setup

and the contact line between liquid and solid, the physical mechanism still remains unclear.

Chung et al. (2004) investigated the effect of circular and square sections on adiabatic two-phase flow in micro capillaries. As the result, it is observed that although only slug and annular flow can be observed, the flow maps for these flow patterns under different liquid and gas speeds show completely different trends. In square microchannels, the flow in the corner may stabilize the total flow field. On the other hand, in circuclar micro channels, the liquid film can evenly spread over the whole perimeter of the tube, making the flow more unstable. So compared to square microchannels, the flow patterns at circular microchannel may vary at lower liquid and gas superficial velocity. From the above research, it is apparent that similar mechanism would also occur in convective boiling.

Therefore, the objectives of this research are: (a) Investigation on convective boiling heat transfer characteristics in a single microchannel through flow visualization with simultaneous measurement of local heat transfer. (b) Investigation of the rules of corners in square microchannels to heat transfer characteristics.

EXPERIMENTAL DEVICE

Figure 1 shows the flow loop used in the present experiments. HCFC123 was employed as a working fluid. A twin plunge pump was employed in most experiments in order to provide mass flux from 100 to 800 kg/m²s. Unlike a single plunge pump, the twin plunge pump keeps a constant flow rate without introducing unwanted bubbles into the test section. The uncertainty interval of the flow rate is within $\pm 1\%$.

Figure 2 shows the test section used in the present experiment. Pyrex glass cylinders with different cross sections are applied. The dimension of the circular cross section is 0.21 mm in inner diameter and 0.4 mm in outer diameter. The dimension of the square cross section is 0.214 mm in hydraulic diameter and 1.8 mm in outer diameter. Note that the outer wall of the square cross section is still circular. So it can provide a perfect shape for the estimation of heat loss.

In order to heat the tube, the mixture of ITO (Indium Tin Oxide) and silver was evenly sputtered on the outer surface of the tube. Fig. 3 shows the SEM picture of the sputtered thin film. The sputtered film thickness was about 100nm. The
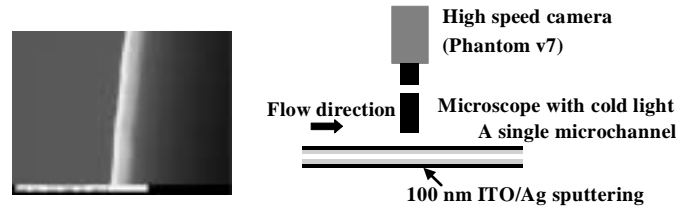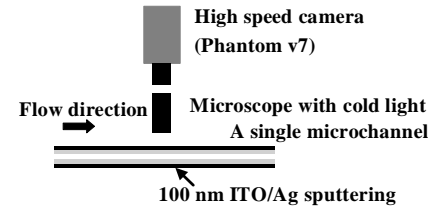
total resistance of the sputtered glass tube was about 1000 Ω. Nine K-type thermocouples of 25 μm OD, calibrated with the accuracy of ± 0.1 K, were glued on the tube outer surface with thermally conductive silicon.

A high-speed CMOS camera (Vision Research, Phantom v7) was employed for the flow visualization inside the microtube. The images having 700x105 pixels were taken at 24000 frames/sec., as shown in fig. 4.

DATA REDUCTION

The heat flux transferred to the working fluid q [W/m²] is calculated as:

$$q(x) = I^2 R(x)/\pi D_i - q_{loss}(x), \qquad (1)$$

where $I^2 R(x)$ corresponds to the Joule heating. The local heat loss from the test section to the environment $q_{loss}(x)$, depends on the outer wall temperature T_{wout} and the environmental temperature T_{air}, and is given by

$$q_{loss}(x) = h_{loss}(T_{wout}(x))(T_{wout}(x) - T_{air}). \qquad (2)$$

Since T_{air} is almost constant, h_{loss} is assumed to be a function of T_{wout}, and determined through a preliminary heating experiment with keeping the test section empty. In the actual convective boiling experiment, the maximum heat losses in all experimental conditions are less than 25% of the total heat generation.

Since there is a very thin deposition layer (100 nm) of ITO and Ag on the outer wall of the tube, an one-dimensional heat conduction equation on cylinder coordinate is necessary to calculate the inner wall temperature, i.e.,

$$T_{win} = T_{wout} - \frac{\ln\left(\frac{D_o}{D_i}\right)q(x)D_i}{2k}, \qquad (7)$$

where T_{wout} represents the outer wall temperature on the inner side of the deposition layer, which can be obtained through another one dimensional heat conduction equation. For the square cross section, D_o is taken as the hydraulic diameter.

Finally, for both glass and metal tubes, the heat transfer coefficient is calculated as:

$$h(x) = \frac{q}{T_{win}(x) - T_{ref}(x)}, \qquad (8)$$

where $T_{ref}(x)$ is the local bulk mean temperature of the refrigerant. When the fluid is in the saturated region, the local bulk mean temperature is equal to the saturation temperature, and is derived from the local pressure distribution $P_{sat}(x)$ described below.

The thermal entrance length (Kays and Crawford, 1993) is within 10 mm under all experimental conditions and there exists about 20 mm before heating section for the entrance of the test section.

The total pressure loss ΔP_{total} in the test section can be decomposed as

$$\Delta P_{total} = \Delta P_{sub} + \Delta P_{sat} + \Delta P_{sup}, \qquad (9)$$

where ΔP_{sub}, ΔP_{sat}, and ΔP_{sup} are the pressure losses in the subcooled liquid, saturated boiling and superheated vapor regions, respectively. The length of the subcooled region l and the pressure loss ΔP_{sub} are calculated as follows. We first assume an arbitrary value for l, and calculate ΔP_{sub} as

$$\Delta P_{sub} = f \frac{1}{2}\rho U^2 \frac{l}{D_i}, \qquad (10)$$

where f, ρ and U are the friction factor of the laminar Poiseuille flow, the liquid density and the bulk mean velocity, respectively. The saturation pressure at $x = l$ is given by

$$P_{sat}(l) = P_{in} - \Delta P_{sub}, \qquad (11)$$

where P_{in} is the inlet pressure. Then, the saturation temperature T_{sat} is calculated from the saturation table of the refrigerant (REFPROP). Finally, the new value of l is obtained from the energy balance, i.e.,

$$\int_0^l q(x)\pi D_i dx = \dot{M} C_p \left(T_{sat}(l) - T_{in}\right). \qquad (12)$$

The iterative calculation using Eqns. (10-12) is repeated until the value of l converges.

The local vapor quality χ in the saturated region is calculated as

$$\chi(x) = \frac{\int_l^x q(x)\pi D_i dx}{\dot{M} h_{lv}}. \qquad (13)$$

The length of the saturated region s is determined from the above integration in such a way that $\chi = 1$ at $x = l+s$. The pressure loss in the superheat region ΔP_{sup} ($l + s < x \le L$) is determined by the laminar flow solution for vapor using physical properties at the local pressure and temperature.

Finally, the pressure loss in the saturated boiling region, ΔP_{sup}, is determined by Eq. (9). The local pressure $P_{sat}(x)$ in the saturated boiling region is assumed to be linearly distributed along the tube, and given by

$$P_{sat}(x) = P_{sat}(l) - \Delta P_{sat}\frac{x-l}{s}. \qquad (14)$$

It is very difficult to define steady state in microchannels because there are always very large fluctuations in pressure and temperature history. However, with the aid of high-speed camera, the definition of steady state can be considered as the appearance of semi-periodic variation of flow patterns, as indicated by Yen et al., 2004. When each period of flow pattern variation becomes similar within $\pm 5\%$, the steady state is considered to be achieved. It usually takes about 20~30 minutes. Temperature and pressure data for the averaged local heat transfer coefficients are taken within an hour for the large variation in flow patterns.

As the same as Yen et al. (2003), the propagation of the componential uncertainties in data reduction error is estimated by ANSI/ASME PTC 19.1 through the data reduction method described above.

In this experiment, only the data in which temperature difference between the inner wall and the working fluid larger than $4^O C$ is taken as reliable experimental data. According to the estimation of including the accuracy of the test sections and experimental devices through data reduction procedure, the final uncertainties for the heat transfer coefficients are still within $\pm 10\%$.

EXPERIMENTAL RESULTS
Semi-periodic variation of flow patterns

In steady state described above, the flow field shows semi-periodic variation of flow patterns in both square and circular cross sections. The period of flow pattern variation varies from 0.08 to 0.12 sec. in both square and circular cross sections under all experimental conditions.

Figs. 5 and 6 show the flow patterns observed in square and circular cross sections. The flow patterns include bubbly, plug, annular and capillary flow patterns. Capillary flow pattern means the independent droplet moving on the inner wall of the test section and it is named by Carey (1996). As evaporation exceeds, liquid film of the annular flow pattern finally splits into independent droplets, forming capillary flow pattern.

Figure 7 shows the ratio of flow pattern history in a period of flow variation at similar experimental conditions except different shapes of cross sections. At low vapor qualities ($\chi\sim$ 0.07), local heat transfer coefficients have larger values in square cross section than in circular cross section and the period of time variation in square cross section ($\tau = 0.1071$ sec.) is larger than that in circular cross section ($\tau = 0.0841$ sec.). The constitution of flow patterns is also simpler in the square microchannel. Capillary flow pattern is not observed. So the flow field is more stable in square microchannels. Notice that the bubbly flow pattern has larger ratio in square cross section.

From the flow visualization, it is observed that in square microchannels, dry-out of liquid film always occur around the center of plane in annular flow pattern. As the evaporation exceeds, the contact line retreats to corners. So the formation of moving droplets becomes very difficult. On the other hand, in circular microchannels, the liquid film distributes evenly on the inner wall. So there is no dry out in annular flow pattern and the thickness of liquid film decreases evenly.
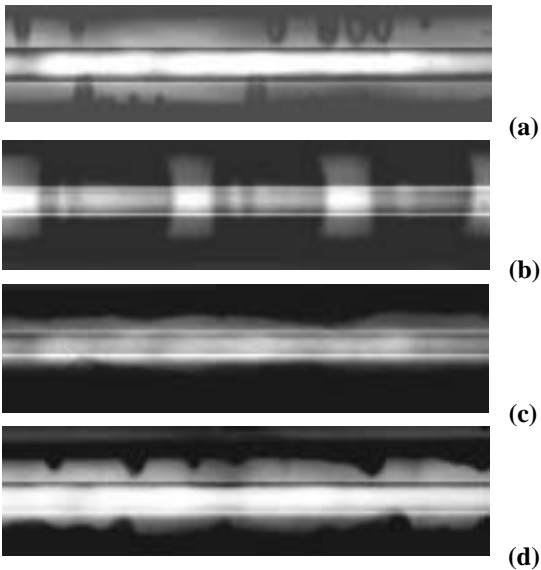
Fig. 5. Flow patterns observed in the 0.214 mm square microchannel. (a)Bubbly flow. (b) Plug flow. (c) Annular flow.
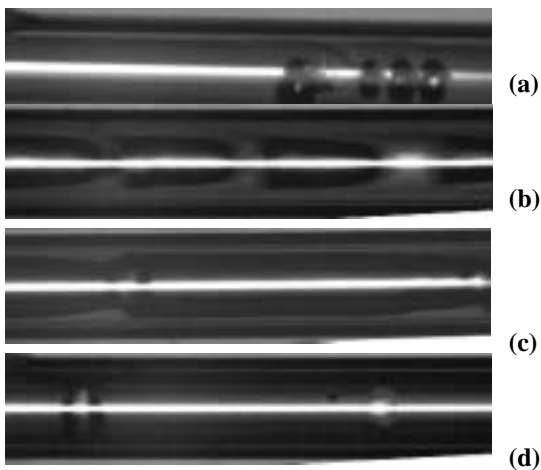

Fig. 6. Flow patterns observed in the 0.21 mm circular microchannel. (a)Bubbly flow. (b) Plug flow. (c) Annular flow. (d) Capillary flow.

However, such even decrease results in the early breakdown of energy balance of molecules of working fluid and surface energy between working fluid and wall. Finally capillary flow pattern forms at the early stage of flow pattern variation and maintains a long time.

On the other hand, at higher vapor qualities ($\chi \sim 0.6$), local heat transfer coefficients become similar. The constitutions of flow patterns are also similar. So it is conjectured that heat transfer coefficients of annular and slug flow pattern are similar in both cross sections. The reason for larger ratio of bubbly flow pattern in square the microchannel will be discussed carefully in the next section.
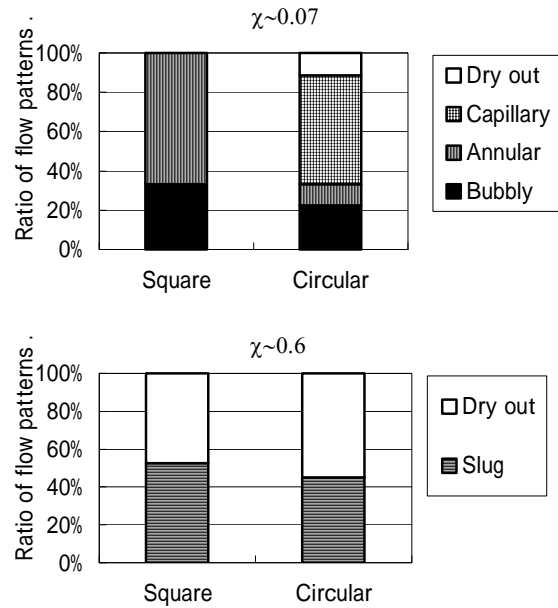

Fig. 7. Ratios of flow patterns in a period under different cross sections at two different vapor qualities. Above: $\chi \sim 0.07$, h=13336 W/m^{2}K for square microchannel and h=5003 W/m^{2}K for circular microchannel. Below: $\chi \sim 0.6$, h=3135 W/m^{2}K for square microchannel and h=2664 W/m^{2}K for circular microchannel.
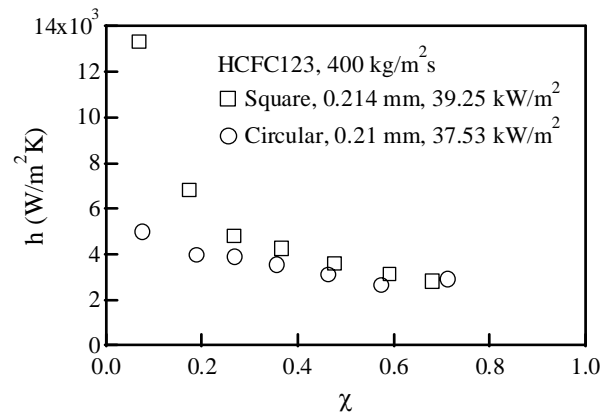

Fig. 8. Local heat transfer coefficients versus vapor quality under different shapes of cross sections with similar experimental conditions.

Heat transfer characteristics

Figure 8 shows the local heat transfer coefficients versus vapor quality under similar experimental conditions except the shapes of cross sections. The local heat transfer coefficients at low and high vapor qualities are simultaneously taken as the same as flow pattern observations in fig. 7. The local heat transfer coefficients decrease with increasing vapor qualities as reported by Yen et al (2003). The local heat transfer coefficients in the square cross section is larger than those in the circular cross section at $\chi<0.4$ and then become similar when $\chi>0.4$ as observed in fig. 6. In square microchannels, corners act as very effective nucleation sites at lower vapor
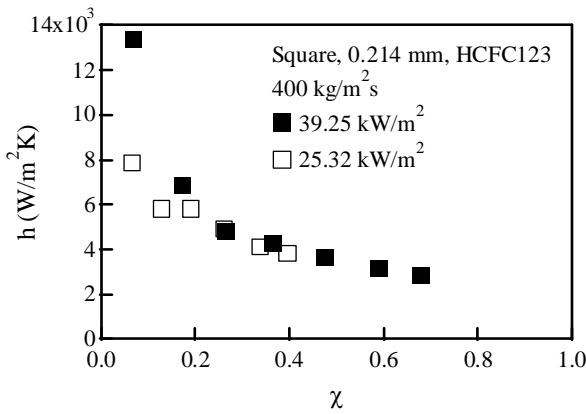
Fig. 9. Local heat transfer coefficients versus vapor quality under different heat fluxes in 0.214mm square mirochannel, medium mass flux.
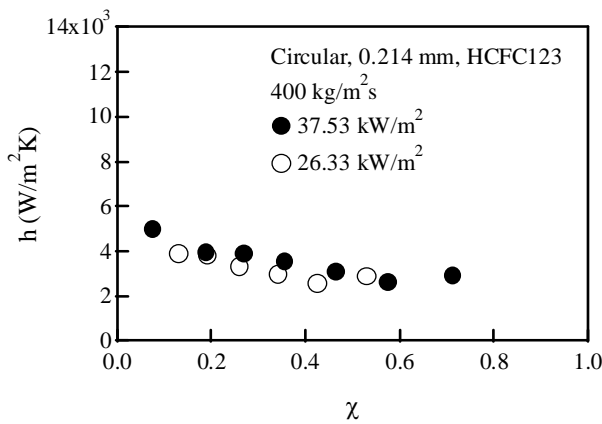

Fig. 10. Local heat transfer coefficients versus vapor quality under different heat fluxes in 0.21mm circular mirochannel, medium mass flux.

Fig. 11. Number of nucleation sites versus boiling number under different cross sections of microchannels.

qualities, enhancing heat transfer coefficients. On the other hand, at higher vapor qualities, the main flow patters becomes slug flow pattern and its heat transfer characteristics seem to be independent of the shape of test section.

Figure 9 shows the local heat transfer coefficients under different heat fluxes in the square microchannel at medium mass flux (400 kg/m²s). When $\chi < 0.3$, higher heat flux results in higher heat transfer coefficients, this is quite different from the experimental results by Yen et al (2003). Fig. 10 shows the local heat transfer coefficients under different heat fluxes in the circular microchannel at the same mass flux (400 kg/m²s). Different from fig. 9, local heat transfer coefficients seems be independent of heat fluxes, as reported by Yen et al., (2003).

By the flow visualization through all positions of the test section at steady state, the number and nucleation frequency of active nucleation sites are carefully investigated to explain the results from figs. 7 to 9. Fig. 11 shows the number of active nucleation cavities versus boiling number observing from all the above experimental runs. It is observed that in square microchannel, the number of nucleation sites increases with
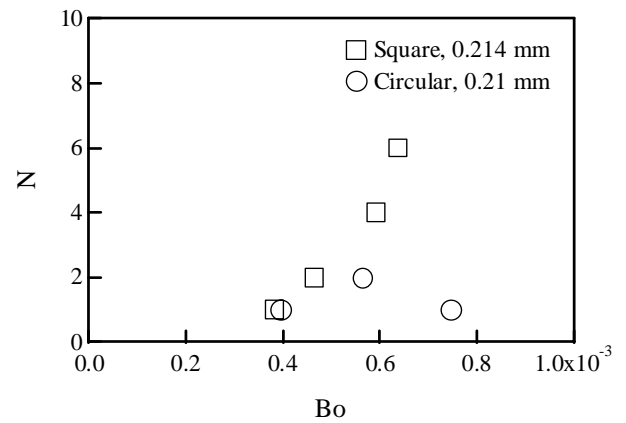
increasing boiling number. On the other hand, in the circular microchannel, the number of nucleation sites is independent of boiling number and there are only 1 to 2 nucleation sites. The independence of nucleation sites to boiling number leads to in independence of local heat transfer coefficients to heat and mass fluxes in circular microchannel. Moreover, it is also observed that in the circular microchannel, the nucleation only occurs at some specific larger cavities in all experimental runs while in the square microchannel, the nucleation sites always change their position under different experimental runs. The very limited nucleation sites also lead to not sufficient nucleation at low vapor quality. Finally it results in the very small dependence of local heat transfer coefficients to vapor qualities.

In contrast to the circular microchannel, the square microchannel has unlimited possible nucleation sites since corners exist. Corners also can enrich the working liquid so that bubble nucleation continues to occur even in plug and annular flow patterns, as shown in fig. 12.

As to the nucleation frequencies, they are similar in both square and circular test sections at the same heat fluxes. From the above investigations, it is conjectured that the number of nucleation sites dominates local heat transfer coefficients at low vapor qualities and corners in square microchannels can serve as very effective nucleation sites. As to circular microchannels, if inner wall is very smooth, there would be no cavities for bubble nucleation and local heat transfer coefficients are mainly the mechanisms of annular and slug flow. In such condition, local heat transfer coefficients become independent of different vapor qualities, heat and mass fluxes.

Although in the square microchannel, heat transfer coefficients increase with increasing nucleation sites, from fig. 13, it is also observed know that heat transfer coefficients very soon reach its maximum because of the very limited space for bubble growth. Fig. 14 shows the high-speed camera photos of bubble expansion in the square microchannel. The space is so limited that only very few of the all nucleation bubbles can grow and expand. This explains the limitation in fig. 13 and explains the existence critical boiling number for maximum heat transfer coefficient exists.
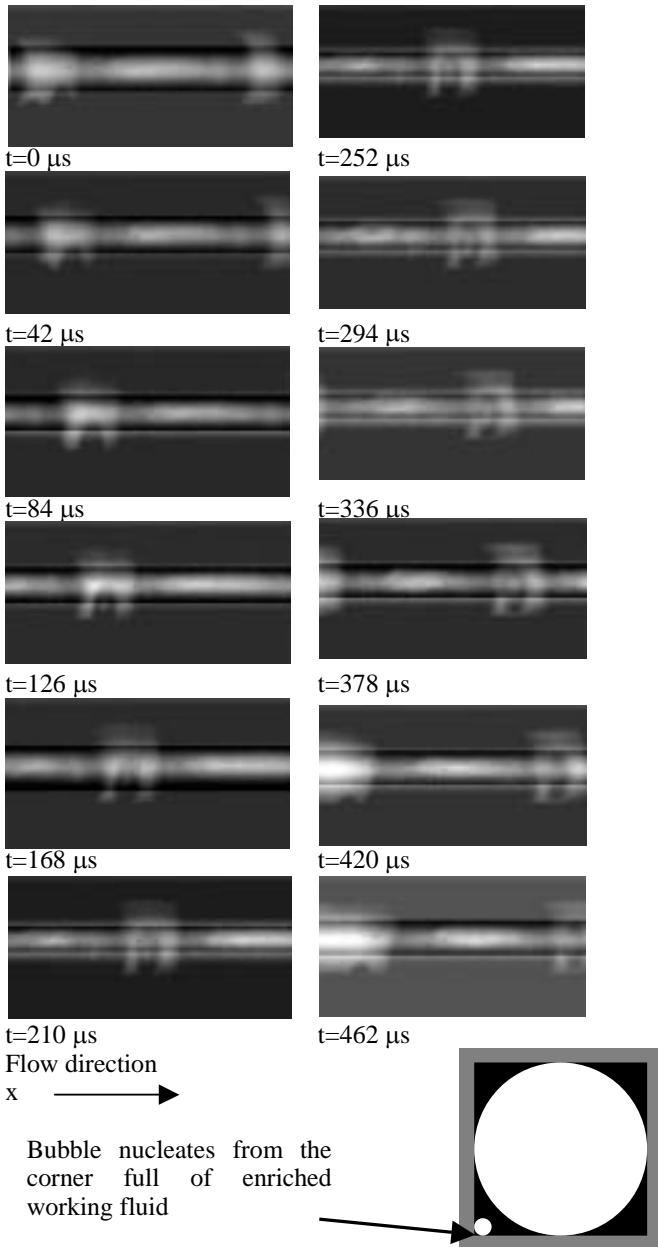
t=0 μs

t=252 μs

t=42 μs

t=294 μs

t=84 μs

t=336 μs

t=126 μs

t=378 μs

t=168 μs

t=420 μs

t=210 μs

t=462 μs

Flow direction

x ⟶

Bubble nucleates from the corner full of enriched working fluid

Fig. 12. Above: Bubble nucleation from the corner in plug flow pattern, 0.214mm square mirochannel. Mass flux: 400 kg/m^{2}s, Heat flux: 39.25 kW/m^2 Vapor quality: 0.21. Below: Description for bubble nucleation in plug slow pattern.

In this experiment, Bo is about 4.5e-4 in the square cross section and less than 4.0e-4 in the circular cross section. This results are quite in proportional to the area of different cross sections. So the critical boiling number is considered to be in proportional to the area of cross section:

$$Bo_{crit} \sim A .$$

Under critical boiling number, active nucleation sites play a very important role to local heat transfer coefficients. However, local heat transfer coefficients become independent of most experimental parameters at experimental conditions higher than the critical *Bo*.
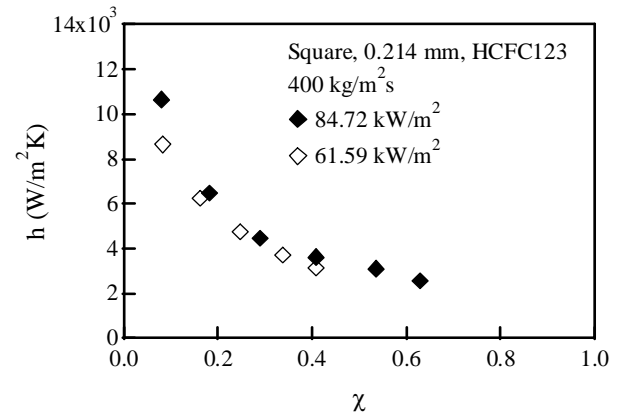

Fig. 13. Local heat transfer coefficients versus vapor quality under different heat fluxes in 0.214mm square mirochannel at high heat and mass fluxes.
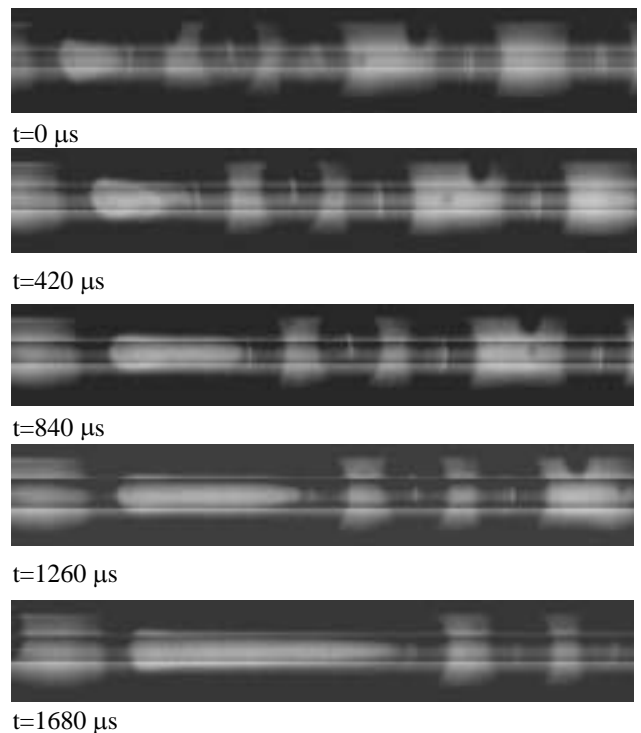

t=0 μs

t=420 μs

t=840 μs

t=1260 μs

t=1680 μs

Fig. 14. Limited number of bubble growth in 0.214mm square mirochannel. Mass flux: 400 kg/m^{2}s, Heat flux: 39.25 kW/m^2 Vapor quality: 0.11.

At high vapor qualities, the flow patterns become only slug and annular flow. So the value of local heat transfer coefficients remains constant (2000~3000 W/m^{2}K) in both circular and square microchannels. The value of 0.5 mm circular titanium tube is also similar to 2000W/m^{2}K (see, Yen et al., 2004). The similar values indicate that slug and annular flow patterns have similar heat transfer mechanism and are less dependent of hydraulic diameters of microchannels.

Pressure losses

Figure 15 shows the pressure time history for both circular and square microchannels. It is observed there exists large
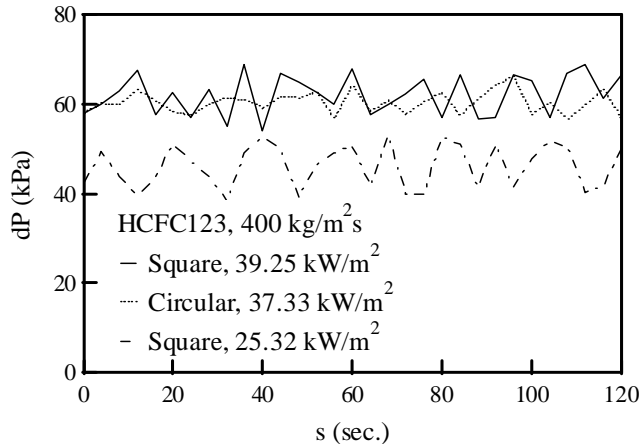
Fig. 15. Time history of pressure loss in square and circular microchannels, 400 kg/m²s.

fluctuations of pressure losses in both circular and square microchannels The amplitude of the pressure fluctuation is about 10 to 15 kPa and it is the results from the semi-periodic flow pattern variation observed in microchannels. Also at similar experimental conditions, the pressure losses are similar in square and circular microchannels.

CONCLUSIONS

The visualization experiments with simultaneous measurement of local heat transfer coefficients under different cross sections of micro conduits were carried out. Semi-periodic variations of flow patterns were observed. Such variation leads to large pressure fluctuations.

Heat transfer characteristics are mainly controlled by nucleation sites. Corners in the square micro channels act as effective active nucleation sites, making much higher heat transfer coefficients than circular conduits. On the other hand, lack of cavities in smooth glass circular microchannel results in relatively smaller heat transfer coefficients. Since both local heat transfer coefficients and time history of flow pattern variations become similar at higher vapor qualities, heat transfer characteristics of slug and annular flow patterns are considered to be similar in both cross sections.

The confined space limits the bubble growth. So there exist maximum heat transfer coefficients and critical boiling number. Critical boiling number is in proportion to area of cross section.

ACKNOWLEDGMENTS

The author would like to thank Prof. Kato in AIST and Mr. Sasaki in Elionix for their helping in SEM photos.

NOMENCLATURES

Bo: boiling number, Bo$=q/(h_{lv}\ \dot{m})$
C_p: specific heat at constant pressure [J/(kg K)]

f : friction factor, $\Delta P_{sub}\Big/\left(\dfrac{1}{2}\rho U^2\dfrac{L}{D_i}\right)$

D_o: outer tube diameter [m]

D_i: inner tube diameter [m]
h_{loss}: heat loss coefficient [W/(m² K)]
h_{lv}: latent heat [J/kg]
h : heat transfer coefficient [W/(m² K)]
I: electric current through the test section [A]
k : thermal conductivity [W/(m K)]
l: axial length of the subcooled liquid region [m]
L: total length of the test section [m]
$\dot{m}$: mass flux [kg/(m²s)]
P_{in}: pressure at the test section inlet [Pa]
P_{sat}: saturated pressure [Pa]
q: heat flux [W/m²]
T_{wout}: outer wall temperature [   ]
T_{win}: inner wall temperature [   ]
t: relative time history of flow patterns[s]
ΔP_{fl} : single phase pressure loss [Pa]
ΔP_{sub}: pressure loss of the subcooled liquid region [Pa]
ΔP_{sup}: pressure loss of the superheated gas region [Pa]
ΔP_{total}: total pressure loss in the test section [Pa]
x: axial coordinate [m]
χ: vapor quality

REFERENCES

Carey, V. P., 1992, Liquid-vapor phase-change phenomena, Hemisphere Publishing Corporation.

Chung, P. M. –Y. and Kawaji, M., 2004. The Effect of Channel Diameter on Adiabatic Two-Phase Flow Characteristics in Microchannels. Int. J. Multiphase Flow. 30, 735-761.

Steinke, M. E., Kandlikar, S. G., 2003. Flow boiling and pressure drop in parallel microchannels. First International Conference on Microchannels and Minichannels, April 24-25.

Mehendale, S. S., Jacobi, A. M., Shah, R. K., 2000. Fluid flow and heat transfer at micro- and meso-scales with application to heat exchanger design. App. Mech. Rev. 53, 175-193.

Kandlikar, S. G., 2004. Heat Transfer Mechanisms During Flow Boiling in Microchannels. Trans ASME: J. Heat Transfer

Kandlikar, S. G., 2002. Fundamental issues related to flow boiling in minichannels and microchannels, Exp. Therm. Fluid Sci. 26, 389-407.

Yen, T. -H., Kasagi, N. Suzuki, Y., 2003. Forced Convective Boiling Heat Transfer in Microtubes at Low Mass and Heat Fluxes. Int. J. Multiphase Flow. 29, 1771-1792.

Yen, T. H., Suzuki, Y., and Kasagi, N.,Visualization of convective boiling in a micro tube with simultaneous measurement of local heat transfer, Proc. 1st Int. Forum Heat Transfer, November 2004, Kyoto, pp. 119-120.

Ravigururajan, T. S., 1998. Impact of channel geometry on two-phase flow heat transfer characteristics of refrigerants in microchannel heat exchangers, Trans ASME: J. Heat Transfer. 120, 485-491.

Saitoh, S., Daiguji, H., Hihara, E., 2000. Boiling heat transfer and pressure drop of HFC134a in horizontal small-diameter tubes. Proc. 39th National Heat Transfer Symp. of Japan, Sapporo, Japan, 667-668.

Serizawa, A., Feng, Z., Kawara, Z., 2002. Two-phase flow in microchannels. Exp. Therm. Fluid Science 26, 703-714.